SMC-TR-04-09

AEROSPACE REPORT NO.
TR-2003(1534)-1

Mechanical Property Characterization of P-5Ag Silver-Filled Carbon

20 December 2003

Prepared by

D. J. CHANG, G. L. STECKEL, and D. N. PATEL
Space Materials Laboratory
Laboratory Operations

Prepared for

SPACE AND MISSILE SYSTEMS CENTER
AIR FORCE SPACE COMMAND
2430 E. El Segundo Boulevard
Los Angeles Air Force Base, CA 90245

Space Systems Group

THE AEROSPACE CORPORATION
El Segundo, California

This report was submitted by The Aerospace Corporation, El Segundo, CA 90245-4691, under Contract No. FA8802-04-C-0001 with the Space and Missile Systems Center, 2430 E. El Segundo Blvd., Los Angeles Air Force Base, CA 90245. It was reviewed and approved for The Aerospace Corporation by P. D. Fleischauer, Principal Director, Space Materials Laboratory; and R. W. Fillers, Principal Director, Space Launch Operations. Lt. Diane Moerer was the project officer for the program.

This report has been reviewed by the Public Affairs Office (PAS) and is releasable to the National Technical Information Service (NTIS). At NTIS, it will be available to the general public, including foreign nationals.

This technical report has been reviewed and is approved for publication. Publication of this report does not constitute Air Force approval of the report's findings or conclusions. It is published only for the exchange and stimulation of ideas.

Diane Moerer

Lt. Diane Moerer
SMC/CLM

REPORT DOCUMENTATION PAGE

Form Approved
OMB No. 0704-0188

1. REPORT DATE (*DD-MM-YYYY*)	2. REPORT TYPE	3. DATES COVERED (*From - To*)
20-12-2003		

4. TITLE AND SUBTITLE

Mechanical Property Characterization of P-5Ag Silver-Filled Carbon

5a. CONTRACT NUMBER
FA8802-04-C-0001

5b. GRANT NUMBER

5c. PROGRAM ELEMENT NUMBER

6. AUTHOR(S)

D. J. Chang, G. L. Steckel, and D. N. Patel

5d. PROJECT NUMBER

5e. TASK NUMBER

5f. WORK UNIT NUMBER

7. PERFORMING ORGANIZATION NAME(S) AND ADDRESS(ES)

The Aerospace Corporation
Laboratory Operations
El Segundo, CA 90245-4691

8. PERFORMING ORGANIZATION REPORT NUMBER

TR-2003(1534)-1

9. SPONSORING / MONITORING AGENCY NAME(S) AND ADDRESS(ES)

Space and Missile Systems Center
Air Force Space Command
2450 E. El Segundo Blvd.
Los Angeles Air Force Base, CA 90245

10. SPONSOR/MONITOR'S ACRONYM(S)
SMC

11. SPONSOR/MONITOR'S REPORT NUMBER(S)
SMC-TR-04-09

12. DISTRIBUTION/AVAILABILITY STATEMENT

Approved for public release; distribution unlimited.

13. SUPPLEMENTARY NOTES

14. ABSTRACT

Silver-filled carbon ring material P-5Ag, produced by Morgan AM&T, Inc., has been used in cryogenic applications. For example, it was used to fabricate carbon ring seals for the Atlas RL10 engine. However, the mechanical properties of this material, i.e., tensile strength and modulus, shear strength and modulus, as well as fracture toughness, have not been well characterized, particularly at the liquid-nitrogen temperature.

A test series was conducted to characterize both the room-temperature and the cryogenic-temperature mechanical properties for silver-filled carbon material P-5Ag. The P-5Ag carbon material was procured from Morgan AM&T, Inc. The types of tests in this series included tensile strength, tensile modulus, shear strength, shear modulus, flexure strength and modulus, mode I fracture toughness, and coefficients of thermal expansion (CTE). However, because of the limited number of tests in each category, highly reliable engineering allowables cannot be established.

15. SUBJECT TERMS
Silver-filled carbon material, Tensile properties, Shear properties, Fracture toughness, Cryogenic temperature

16. SECURITY CLASSIFICATION OF:			17. LIMITATION OF ABSTRACT	18. NUMBER OF PAGES	19a. NAME OF RESPONSIBLE PERSON
a. REPORT	b. ABSTRACT	c. THIS PAGE			Dick Chang
UNCLASSIFIED	UNCLASSIFIED	UNCLASSIFIED		23	19b. TELEPHONE NUMBER (*include area code*) (310)336-5808

Acknowledgments

The project was funded by the Aerospace Medium Launch Vehicles (MLV) Atlas program office at The Aerospace Corporation under the U. S. AF contract F04701-93-C-0094. Dr. Robert W Fillers, Principal Director of Medium Launch Vehicles Directorate, authorized the project. Mr. Randall L. Williams was the technical monitor.

The authors wish to thank Mr. Robert M. Castaneda for conducting the thermal expansion tests, Mr. Ben Nelson for assistance with the flexure and fracture toughness testing, and Mr. George W. Henderson for performing optical microscopy. Mr. Paul Adams is acknowledged for X-ray diffraction and electron microscopy analyses.

Contents

Figures

Tables

1. Background

Silver-filled carbon ring material P-5Ag, produced by Morgan AM&T, Inc., has been used in cryogenic applications. For example, it was used to fabricate carbon ring seals for the Atlas upper stage engine. However, the mechanical properties of this material, i.e., tensile strength and modulus, shear strength and modulus, as well as fracture toughness, have not been well characterized, particularly at the liquid-nitrogen temperature. A test series was initiated to characterize both the room-temperature and the cryogenic-temperature mechanical properties for this material. The experimentally measured properties will enable the analysts to more accurately assess the structural integrity of the carbon seals under operational conditions.

2. Experimental Procedures

2.1 Specimen Configurations

Three types of Ag/carbon starting materials were procured. They were dog-bone-shaped specimens, rectangular bars, and cylindrical rods. Dog-bone-shaped specimens were used for tensile strength testing. Rectangular specimens were used for flexure and coefficient of thermal expansion (CTE) testing. Cylindrical rods were used for torsion testing and microstructural evaluations. Table 1 shows the sizes of the specimens associated with each of the five types of property measurements: tension, flexure, torsion, fracture toughness, and CTE. The mechanical tests were conducted at room temperature and in liquid nitrogen (–320°F), and the CTE was measured from –240 to +210°F.

For strength testing, the tensile specimens had an initial gage width of 0.50 in., and the torsion specimens had an initial gage diameter of 0.375 in. The gage width of the tensile specimens was subsequently reduced to 0.25 in., and the gage diameter of the torsion specimens was reduced to 0.25 in. to ensure that the failure would occur in the gage area. For modulus testing, the 0.50-in. width and 0.375-in. diameter were used in tension and torsion, respectively, to provide sufficient space for strain gage mounting. There were no strain gages mounted for the strength specimens.

Table 1. Specimen Geometrical Configurations

Type of Testing	Length (in.)	Width (in.)	Thickness (in)	Type of Specimen
Tensile Strength	4.5	0.50 in. gage width	0.25	Rectangular dog-bone
Tensile Modulus	4.5	0.75	0.25	Rectangular Piece
Torsion Strength	4	0.25 in. gage dia		Cylindrical Rod
Torsion Modulus	4	0.375 in. dia		Cylindrical Rod
Flexure Modulus & Strength	2.5 or 4.5	0.50 or 0.75	0.19 or 0.25	Rectangular Piece
Fracture Toughness	4.5	0.75	0.19	Rectangular Piece
CTE	0.25-0.6	0.25	0.25	Rectangular Piece

2.2 Tensile Testing

A special loading fixture was designed and fabricated for the tensile testing as shown in Figure 1. The tensile dog-bone specimens were supported at the ends of the reduced section between rollers. The rollers transferred tensile loads into the specimens. The fixture eliminated the use of loading pins and adhesive bonding and minimized the occurrence of localized failures in the support area. For tensile modulus measurements, Micro-Measurement EA-06-062TT-350 0/90° strain gages were mounted on the surface of the dog-bone specimens to measure the axial and lateral strains. Tensile testing was conducted using an Instron testing machine.

For the –320°F cryogenic testing, two concentric stainless-steel containers were fabricated and assembled together. The inner container was filled with liquid nitrogen into which the entire length of the specimen was submerged. A special type of insulation powder was filled between the inner and the outer walls of the containers to reduce the thermal loss from the inner container. A sketch of the specimen, the loading fixture, and the container is depicted in Figure 1. After filling the inner container with liquid nitrogen, testing was delayed for a minimum of five minutes to allow the specimen temperature to reach an equilibrium state.

2.3 Torsion Testing

The torsion tests were conducted on an Instron testing machine with a torsion load cell. It was first planned to have the ends of the cylindrical rods gripped by a three-blade chuck. However, we were concerned that slippage between the chuck blade and the specimen would occur if the specimen ends were not tightly chucked. We were equally concerned that the ends would be crushed if the chucking was too tight. To alleviate this problem, aluminum extension parts were fabricated. One end of the extension has a triangular recess that fits the end of the specimens that was machined into a triangle-shaped cross section. The other end had a triangular cross section that was gripped by the chuck. Figure 2 shows the design of the ends for the torsion specimens.

A similar double-wall container for the cryogenic tensile test was also used for the –320°F cryogenic torsion test as shown in Figure 3.

For torsion modulus specimens, Micro-Measurement SK-06-250TM-350 0/90° strain gages were mounted in the gage area on the surface of the 0.375-in.-dia. cylindrical rod. The strain gages were

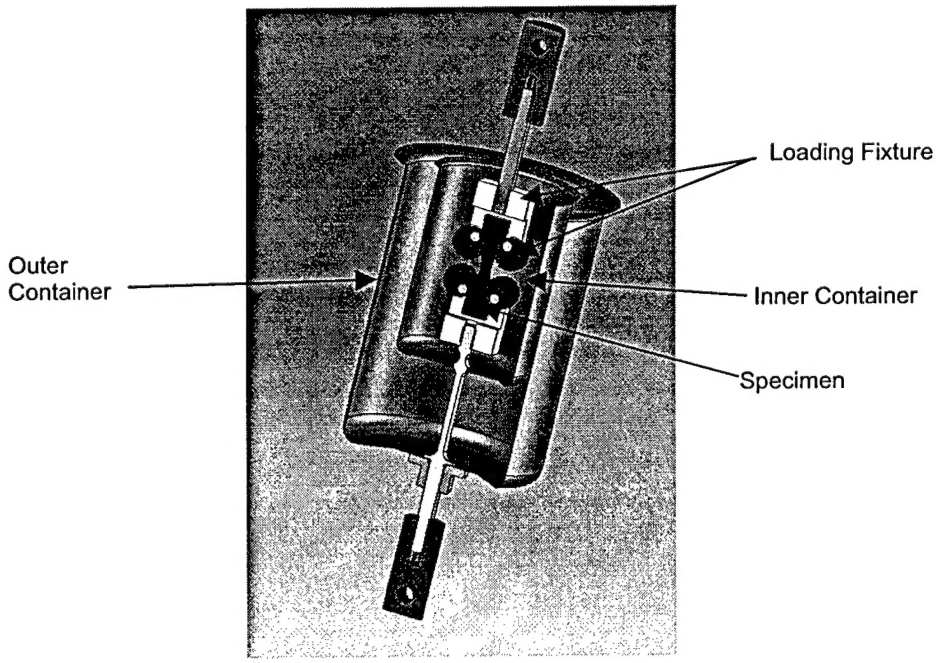

Figure 1. Sketch of tensile test assembly.

mounted at ±45° from the longitudinal axis of the rod, allowing the recording of tensile and compressive strains at ±45° from the pure shear stress plane. Since the strain gages needed large enough surface area and since the failures of the specimen were not needed, the diameter of the cylindrical rod (0.375 in.) was not reduced. For torsion strength specimens, the specimen diameter was reduced to 0.25 in. to ensure that the failures would occur in the gage section.

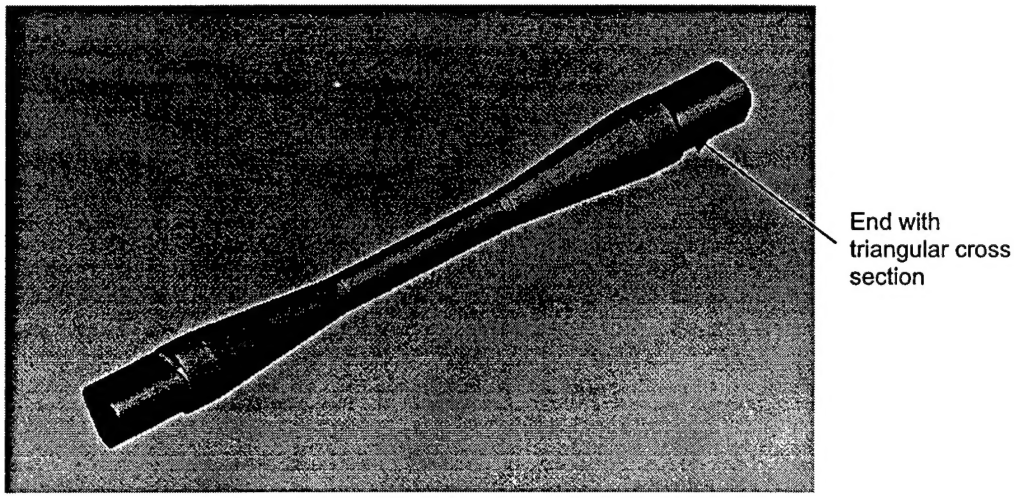

Figure 2. Torsion specimen.

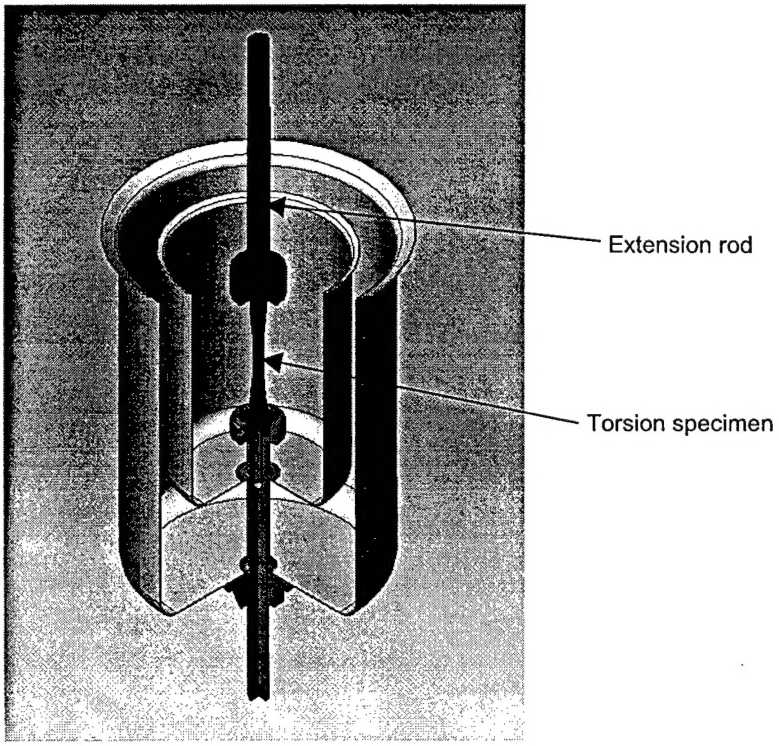

Figure 3. Cryogenic torsion test fixture.

2.4 Flexure Testing

Three-point and four-point bend testing were performed following procedures consistent with the requirements of ASTM D 790, Standard Test Methods for Flexural Properties of Unreinforced and Reinforced Plastics and Electrical Insulating Materials.[1] Test Method I, in which the test sample rests on two supports and is loaded by means of a loading pin midway between the supports, was used for the three-point bend tests. Test method II, in which the sample rests on two supports and is loaded by two loading pins, which are equal distances from the respective adjacent support pins, was used for the four-point bend tests. The distance between the two loading pins (1.0 in. for this study) is either one-third or one-half the support span distance. A fully adjustable support fixture was used so that the distance between the support pins could be set at any desired position. All tests were conducted using 0.250-in.-dia loading pins and support pins.

A minimum support span-to-sample thickness ratio (L/d) of at least 16:1 is generally recommended by ASTM D 790[1] in order to obtain valid modulus data for isotropic materials. For anisotropic materials, such as fiber-reinforced composites, higher L/d ratios are often required. Although P-5Ag is believed to be isotropic, preliminary tests were performed on samples having L/d ratios that varied from 8 to 22 in order to determine the minimum L/d ratio required to obtain valid modulus data. For three-point bend tests, the support span was adjusted between 2.2 and 4.0 in., while the sample thickness was varied between 0.25 and 0.185 in. For four-point bend tests, the support span was adjusted between 2.0 and 3.0 in., while the sample thickness was varied between 0.25 and 0.188 in.

The bend tests were conducted using an Instron Universal Testing Machine having a screw-driven crosshead. All tests were conducted at a constant crosshead speed, i.e. midpoint displacement rate, of 0.05 in./min. Load data were recorded as a function of time using a strip chart and were also recorded with a computer data acquisition system. Midpoint displacement was calculated from the crosshead speed. The instantaneous maximum stress and strain at the surfaces of the samples at midspan were calculated using the standard beam theory expressions for a homogeneous, elastic material given in Table 2 for the three test configurations.

In these equations, P is the instantaneous load, L is the support span, b is the beam width, d is the beam depth (thickness), and δ is the instantaneous deflection at the midspan position. The flexural modulus was determined by a linear regression of the stress-strain data over the steepest initial straight-line portion of the stress-strain curve. For the samples tested in this investigation, the stress-strain curve was linear up to failure, except for an initial nonlinear region. Thus, the linear regression for the modulus fit was usually performed from the onset of linearity to sample fracture.

Table 2. Equations for Stress and Strain for Three-Point and Four-Point Bend Tests

Test Type	Max. Stress	Max. Strain
3-Point Bend	$3PL/2bd^2$	$6\delta d/L^2$
4-Point Bend (Load Span = L/3)	PL/bd^2	$4.7\delta d/L^2$
4-Point Bend (Load Span = L/2)	$3PL/4bd^2$	$4.36\delta d/L^2$

In order to make accurate strain measurements, and hence accurate flexural modulus measurements from midpoint deflection values that are calculated from the crosshead rate, deformations or slack within the loading system must be negligible relative to the sample deflections. In other words, the system stiffness must be very high relative to the sample bending stiffness. In order to verify that this condition was met, initial measurements were made on a 6061 aluminum beam. A flexural modulus of 9.5 msi was measured for the aluminum beam, which agrees very well with the handbook value for 6061 aluminum of 10.0 msi. The aluminum beam had a higher bending stiffness than any of the samples tested in this study. Thus, the assumption that accurate sample strain measurements could be made from the crosshead displacement rate was validated.

In order to further validate the calculation of sample surface strain from crosshead displacement, two four-point bend samples were instrumented with strain gages. Four-point bend samples were selected for strain gages because they have uniform surface strain between the two loading pins, and strain gages can be applied to the compression side of the beam without interfering with the loading pins. One Micro-Measurement Type EA-06-062TT-350 0/90° strain gage was applied to both sides of the samples. Young's modulus and Poison's ratio were determined from the strain gage data for the tensile and compressive sides of the bend samples.

The objectives of these tests were to determine the flexural modulus and the flexural strength. It was assumed that flexural failure would initiate on the tensile side of the beam samples. Therefore, an additional objective was to compare the tensile data and bend data to determine whether flexural testing could be used to determine tensile strength for Ag/carbon.

2.5 Fracture Toughness Testing

Three-point bend testing was used for generating fracture toughness values. 0.75-in.-wide by 0.25-in.-thick beams with a 4.0-in. span were used for these tests. The samples were precracked using a 0.010-in.-thick slitting saw to cut across the sample width at the midspan position on the tensile side. Four samples were tested at room temperature with two samples having a crack depth of 0.040 in. and the other two having a crack depth of 0.080 in. Four samples having a crack depth of 0.080 in. were tested in liquid nitrogen. All fracture toughness samples were tested following the same procedures that were used for the three-point bend tests.

The fracture toughness, K_{1C}, was calculated from the failure load for the cracked specimens by applying the equation,

$$K_{1C} = S(\pi a)^{1/2} F(a/d), \tag{1}$$

where S is the maximum surface stress at the midpoint of the beam, a is the crack depth, and F(a/d) is a geometric factor that depends on the crack depth/beam thickness ratio (a/d) and on the support span/beam thickness ratio (L/d).

2.6 Coefficient of Thermal Expansion (CTE) Measurements

CTE measurements were made using a TA Instruments, Inc. Model No. 2940 Thermal Mechanical Analyzer (TMA). CTE measurements are made with the sample resting on a quartz stage with a quartz probe contacting the upper surface. The quartz probe is attached to a linear variable differential transducer (LVDT), which has a measurement sensitivity of 0.1 μm. The stage is surrounded by a cryostat/furnace assembly. For Ag/carbon, samples approximately 0.25–0.6 in. long and 0.25 in. square were machined from a 2.0 x 0.5 x 0.25 in. rectangular piece of as-received material. CTE measurements were made parallel to length, width, and thickness of the rectangular piece. An initial length measurement was made at room temperature. The samples were then cooled to –150°C (–238°F). Length measurements were made at a rate of 30 points/min as the samples were heated at 5°C/min from –150 to +100°C (–238 to 212°F).

2.7 Microstructural Evaluation

Cross sections from a piece of the 0.375-in.-dia rod stock of Ag/carbon were mounted and polished for optical microscopy and scanning electron microscopy (SEM). Energy dispersive analysis of X-rays (EDAX) was used for chemical analyses of various features observed in the SEM images. X-ray diffraction was used to further evaluate the chemistry and structure of the Ag/carbon material.

Image analysis techniques were employed to estimate void volume within the Ag/carbon material. Scion Image Release Beta 3b by Scion Corporation was used to perform the image analysis on optical micrographs. With this technique, a density slice analysis is performed to highlight void areas, which appear as very dark contrast regions on the digital images. The software counts the number of pixels within the void areas, and the void volume fraction is determined by dividing by the total number of pixels in the image.

3. Results and Discussion

3.1 Tensile Tests

All the room-temperature test data are summarized in Table 3. Initially, 0.5-in.-wide specimens were used for strength testing. As seen from Table 3, all 0.5-in.-wide specimens failed in the loading pin area that gave lower bound strength values. Even when one specimen was tested with a width of 0.375 in., failure still occurred in the loading pin area. When the width was reduced to 0.25 in., the failures shifted to the gage section. The failure data of three specimens, AGFCT6RT, AGFCT8RT, and AGFCT13RT, gave an average of failure strength of 7.32 ksi with a standard deviation of 0.45 ksi. The specimen AGFCT5RT failed prematurely and was not used in the strength population.

Specimens AGFCT1RT, AGFCT2RT, and AGFCT3RT had rosette strain gages for the determination of Young's modulus and Poisson's ratio. Good strain data were obtained from AGFCT1RT and AGFCT2RT. An average modulus of 3.15 msi was obtained from the data for these two specimens. The modulus values were obtained from linear regression analysis of the stress-strain data. Poisson's ratio was determined for specimen AGFCT1RT. Poisson's ratio increased from 0.07 to 0.13 as the tensile stress increased.

Figure 4 depicts a typical tensile stress-strain curve for the material at room temperature. There is a nonlinear response for stresses below 2000 psi. The modulus values were obtained from linear portion of the stress-strain curve.

Table 3. Room-Temperature Tensile Test Results

Specimen ID	Specimen (width x thick., in.)	Failure Load (lb)	Failure Stress (ksi)	Young's Modulus (msi)	Instrumentation	Remarks
AGFCT1RT	0.5x0.25	566	4.528	3.150	One rosette strain gage	See Note 1
AGFCT2RT	0.5x0.25	621	4.968	3.142	Only axial gage working	See Note 1
AGFCT3RT	0.5x0.25	490	3.920	NA	Two rosette strain gages	See Note 1
AGFCT4RT	0.375x0.25	570	6.080	-	No gages	See Note 1
AGFCT5RT	0.249x0.25	291	4.589	-	No gages	See Note 2
AGFCT6RT	0.2515x0.25	428	6.807	-	No gages	See Note 2
AGFCT7RT	0.251x0.25	443	7.043	-	No gages	See Note 1
AGFCT8RT	0.25x0.25	477	7.632	-	No gages	See Note 2
AGFCT13RT	0.209x0.25	393	7.522	-	No gages	See Note 2

Note 1: Specimen failed under loading pins.

Note 2: Specimen failed in mid section.

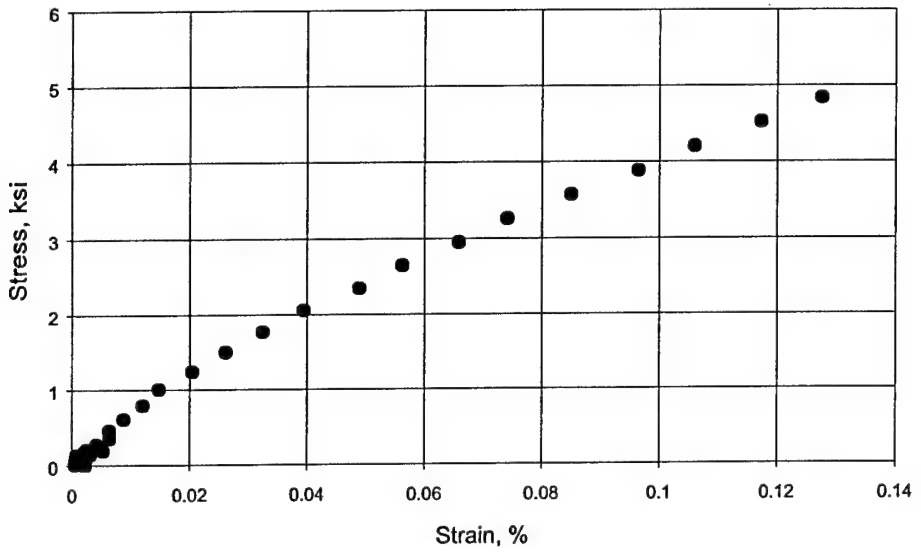

Figure 4. Stress vs. strain curve for specimen AGFC2RT tested at room temperature.

The quarter-bridge lay-out in the Wheatstone bridge circuit that was used in the room-temperature tensile tests did not function satisfactorily for the liquid nitrogen tests due to the large resistance change of the strain-gage foil from room temperature to –320°F. A half-bridge lay-out in the circuit had to be utilized. This involved the use of two identical strain gages (one on the specimen as the active gage, and the other one un-bonded as a dummy), each one serving as a quarter-bridge of the circuit. When both samples were submerged in liquid nitrogen, thermally induced strains were cancelled out, allowing load-induced strains to be measured. However, the liquid-nitrogen strain data were very noisy. The fluctuations were so large that the accuracy of the data was compromised for some tests. For some cases, no usable data could be reduced. Figure 5 shows the load, axial, and transverse strain data for specimen AGFCT18LN, which gave useful strain data. It can be seen that the load vs. time data are smooth. However, the strain vs. time data are very noisy.

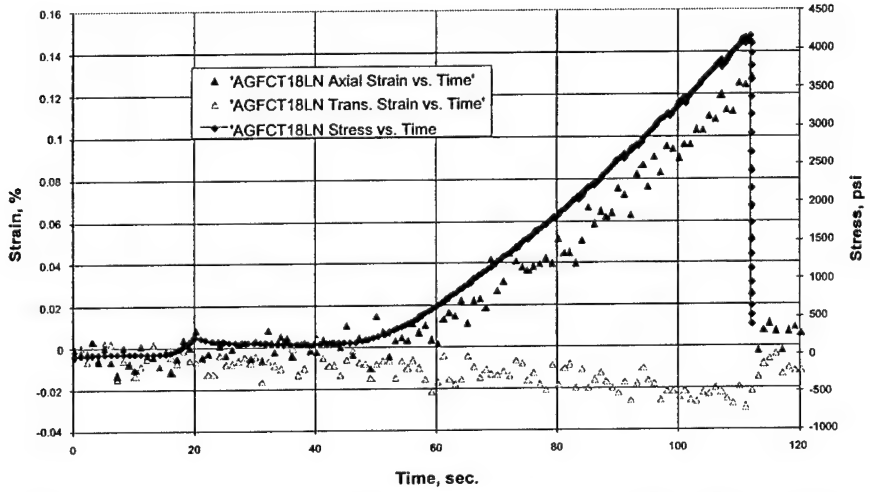

Figure 5. Load, axial, and transverse strain data for specimen AGFCT18LN.

The tensile data for the liquid-nitrogen submersion (–320°F) are shown in Table 4. The average maximum tensile strength from the four liquid-nitrogen temperature specimens, AGFCT9LN, AGFCT11LN, AGFCT12LN, and AGFCT14LN, was 7.23 ksi with a standard deviation of 1.54 ksi. The average tensile modulus value was 3.18 msi from specimens AGFCT16LN-2-SG and AGFCT18LN-2-SG.

The liquid-nitrogen temperature strength and Young's modulus values were very close to the room-temperature values. From a practical point of view, they were identical.

Table 4. Liquid-Nitrogen (–320°F) Tensile Test Results

Specimen ID	Specimen (width x thick., in.)	Failure Load (lb)	Failure Stress (ksi)	Young's Modulus (msi)	Instrumentation	Remarks
AGFCT9LN	0.25 x 0.25	561	8.976	-	No gages	Failed in mid section
AGFCT10LN	0.25 x 0.25	-	-	-	No gages	Specimen failed before loading
AGFCT11LN	0.25 x 0.25	364	5.824	-	No gages	Failed in mid section
AGFCT12LN	0.25 x 0.25	378	6.048	-	No gages	Failed in mid section
AGFCT14LN	0.25 x 0.25	505	8.080	-	No gages	Load dropped once at 390 lb. Failed in mid section
AGFCT15LNT	0.25 x 0.30		0			
AGFCT16LN-2	0.25 x 0.50	683	5.464	2.83	Half bridge rosette	Failed in grip area
AGFCT17LN-2	0.25 x 0.51	490	3.920	NA	Half bridge rosette	Failed in grip area
AGFCT18LN	0.25 x 0.52	520	4.160	3.54	Half bridge rosette	Failed in grip area

3.2 Torsion Tests

All the room-temperature test data are summarized in Table 5. The maximum room-temperature shear strength, averaged from the seven specimens AGFCTQ1RT, AGFCTQ2RT AGFCTQ3RT, AGFCTQ4RT, AGFCTQ5RT, AGFCTQ6RT, and AGFCTQ7RT is 8.32 ksi with a standard deviation of 1.89 ksi. The shear strength is higher than the room-temperature tensile strength of 7.32 ksi. This is reasonable because the material tensile strength is lower than the compressive strength, and the pure shear loading is equivalent to a biaxial stress state in which tension is acting in one direction and compression in the 90° direction.

The average shear modulus value is 1.49 msi from specimens AGFCTQ1RT-SG, AGFCTQ2RT-SG, and AGFCTQ3RT-SG. The standard deviation is 0.22 msi. Since the P-5Ag material is believed to be isotropic, the room-temperature Poisson's ratio can be calculated from the 3.25 msi Young's modulus and the 1.49 msi shear modulus. The calculated Poisson's ratio is 0.09.

For the liquid-nitrogen testing, the shear strength from the three specimens, AGFCTQ4LN, AGFCTQ5LN, and AGFCTQ6LN, was 10.95 ksi with a standard deviation of 0.77 ksi. This value is much higher than the 8.32 ksi measured at room temperature. The average shear modulus in liquid nitrogen was 1.49±0.63 msi from specimens AGFCTQ2LN-SG, AGFCTQ3LN-SG, and AGFCTQ4LN-SG. This is identical to the room-temperature value. The calculated Poisson's ratio is 0.067. The data are summarized in Table 6.

Table 5. Room-Temperature Torsion Test Results

Specimen ID	Specimen (Gage Length x Dia.)	Max. Torque (ft-lb)	Failure Shear Stress (ksi)	Shear Modulus (msi)	Instrumentation	Notes
AGFCTQ1RT	3.15" gage length 0.249" dia at mid point	2.450	9.70	-	No strain gage	Specimen failed
AGFCTQ2RT	3.15" gage length 0.252" dia at mid point	2.455	9.38	-	No strain gage	Specimen failed
AGFCTQ3RT	3.15" gage length 0.25" dia at mid point	2.210	8.64	-	No strain gage	Specimen failed
AGFCTQ4RT	3.15" gage length 0.25" dia at mid point	1.734	6.79	-	No strain gage	AGFCTQ3-CAL Specimen failed
AGFCTQ5RT	3.15" gage length 0.25" dia at mid point	1.267	4.95	-	No strain gage	AGFCTQ4-CAL Specimen failed
AGFCTQ6RT	3.15" gage length 0.25" dia at mid point	2.679	10.48	-	No strain gage	AGFCTQ5-CAL Specimen failed
AGFCTQ7RT	3.15" gage length 0.25" dia at mid point	2.121	8.30	-	No strain gage	AGFCTQ6-CAL Specimen failed
AGFCTQ1RT-SG	3.15" gage length 0.375" dia at mid point	7.413	8.59	1.560	Strain gage	No failure
AGFCTQ2RT-SG	3.15" gage length 0.375" dia at mid point	6.447	7.47	1.550	Strain gage	No failure
AGFCTQ3RT-SG	3.15" gage length 0.375" dia at mid point	2.100	-	1.364	Strain gage	No failure

Table 6. Liquid-Nitrogen Temperature Torsion Test Results

Specimen ID	Specimen (Gage Length x Dia.)	Max. Torque (ft-lb)	Failure Shear Stress (ksi)	Shear Modulus (msi)	Instrumentation	Notes
AGFCTQ4LN	3.15" gage length 0.25" dia at mid point	3.024	11.83	-	No strain gage	Failed at mid section of min. dia
AGFCTQ5LN	3.15" gage length 0.25" dia at mid point	2.660	10.40	-	No strain gage	Failed at mid section of min. dia
AGFCTQ6LN	3.15" gage length 0.25" dia at mid point	2.712	10.61	-	No strain gage	Failed at mid section of min. dia
AGFCTQ2LN-SG	3.15" gage length 0.375" dia at mid point	7.338	8.50	1.571	Strain gage	Failed at grip area
AGFCTQ3LN-SG	3.15" gage length 0.375" dia at mid point	7.765	9.00	1.465	Strain gage	Failed at grip area
AGFCTQ4LN-SG	3.15" gage length 0.375" dia at mid point	8.413	9.75	1.440	Strain gage	Failed at grip area

3.3 Flexure Tests

The results of the three-point and four-point bend tests are summarized in Table 7. The initial tests, S1-S5 and L1-L8, were conducted to determine the minimum L/d ratio necessary to obtain valid modulus data. The flexural modulus calculated from crosshead displacement is plotted as a function of L/d ratio in Figure 6. The plot shows that the flexural modulus increased rapidly for three-point and four-point bend tests as the L/d ratio was increased from approximately 8 to 16. Further increasing the L/d ratio to approximately 21 for three-point bend tests did not result in any additional

Table 7. Flexure Properties of Ag-Carbon at 72° and –320°F.

Sample No.	Width (in.)	Thickness (In.)	Test Type	Span (in.)	Span/Thick Ratio	4-Point Span Ratio	Flexural Modulus (msi)	Flexural Strength (ksi)	Failure Strain (%)
Tested at Room Temperature									
S1	0.501	0.251	4-Point	2.0	8.0	2.0	1.83	8.19	0.52
S2	0.501	0.251	4-Point	2.0	8.0	2.0	2.03	6.84	0.41
L1	0.751	0.250	4-Point	3.0	12.0	3.0	2.66	8.23	0.32
L6	0.750	0.188	4-Point	3.0	16.0	3.0	2.99	8.08	0.28
L7	0.749	0.184	4-Point	3.0	16.3	3.0	3.20	9.51	0.31
L8	0.749	0.188	4-Point	3.0	16.0	3.0	3.26	9.05	0.29
L22	0.751	0.189	4-Point	3.0	15.9	3.0	3.56		
L23	0.751	0.189	4-Point	3.0	15.9	3.0	3.58		
S3	0.501	0.251	3-Point	2.2	8.8	NA	2.37	12.7	0.57
S4	0.501	0.251	3-Point	2.2	8.8	NA	2.35	11.3	0.53
S5	0.501	0.251	3-Point	2.2	8.8	NA	2.44	10.5	0.47
L2	0.750	0.251	3-Point	4.0	15.9	NA	3.12	12.0	0.40
L3	0.750	0.251	3-Point	4.0	15.9	NA	3.21	11.7	0.38
L4	0.750	0.188	3-Point	4.0	21.3	NA	3.12	10.8	0.35
L5	0.750	0.185	3-Point	4.0	21.6	NA	3.19	12.4	0.39
Tested in Liquid Nitrogen									
L18	0.750	0.250	3-Point	4.0	16.0	NA	2.62	11.7	0.44
L19	0.750	0.251	3-Point	4.0	15.9	NA	2.66	12.8	0.48
L20	0.750	0.251	3-Point	4.0	15.9	NA	3.30	12.1	0.40
L21	0.749	0.251	3-Point	4.0	15.9	NA	3.27	13.4	0.44
Average 4-Point Properties at Room Temp. for L/d ≥ 15.9							3.32	8.88	0.29
St. Dev.							0.25	0.73	0.02
Average 3-Point Properties at Room Temp. for L/d ≥ 15.9							3.16	11.7	0.38
St. Dev.							0.05	0.7	0.02
Average 3-Point Properties in Liquid Nitrogen for L/d ≥ 15.9							2.96	12.5	0.44
St. Dev.							0.37	0.8	0.03

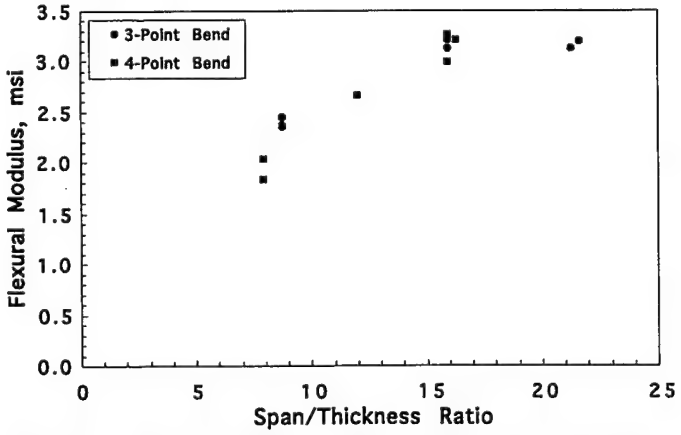

Figure 6. Flexural modulus versus L/d ratio for flexure tests.

increase in flexural modulus. It was concluded that a minimum L/d ratio of 16 was required to obtain valid modulus data for P-5Ag Ag/carbon. All subsequent tests were conducted at an L/d ratio of 16.

The flexural strength data in Table 7 also increased with L/d ratio for the four-point bend tests, but did not vary with L/d ratio for three-point bend tests. It was concluded that average properties should be calculated using only samples having an L/d ratio ≥15.9. At room temperature, the average flexural modulus was 3.32±0.25 msi for four-point bend tests and 3.16±0.05 msi for three-point bend tests. The average room-temperature strength was 8.88±0.73 ksi for four-point bend and 11.7±0.7 ksi for three-point bend tests. Thus, the flexural modulus was equivalent for three-point and four-point bend tests, but the average flexural strength was 30% higher for three-point than for four-point bend tests.

In liquid nitrogen, the average flexural modulus and strength were 2.96±0.37 msi and 12.5±0.8 ksi, respectively, for three-point bend tests. Thus, there were no significant differences between the room-temperature and liquid-nitrogen modulus or strength for three-point bend tests. This is consistent with the tensile test results.

Flexural stress-strain curves are shown in Figure 7 for the room-temperature three-point bend tests. These curves are also representative of the room-temperature four-point bend tests and liquid-nitrogen three-point bend tests. The curves show a small amount of nonlinearity at very low strains, which is probably associated with seating of the samples on the support pins. Otherwise, the curves are linear up to fracture, indicating brittle fracture with no evidence of plastic deformation. The flexural modulus was calculated over the strain range of 0.1 to 0.3% strain.

Four-point bend Sample Nos. L22 and L23 in Table 7, which were not tested to failure, had biaxial strain gages bonded to the tensile and compressive sides of the beams. The flexural moduli,

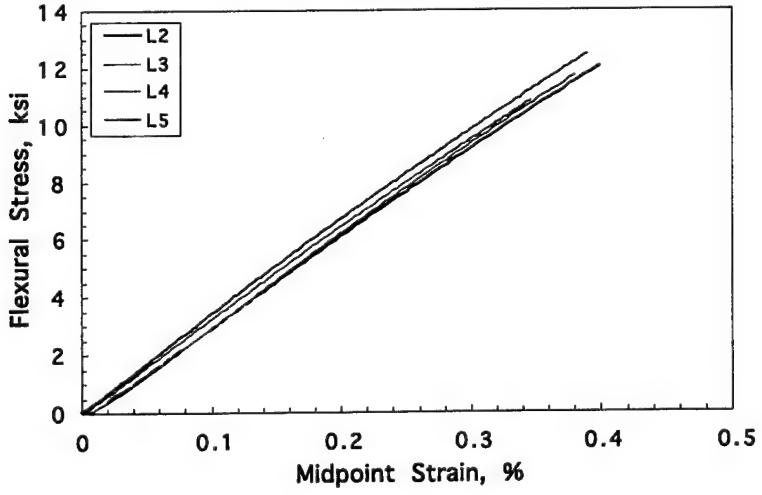

Figure 7. Three-point bend stress-strain curves at room temperature.

calculated from the tensile gage data, compression gage data, and from crosshead displacement are tabulated in Table 8 along with the calculated Poisson's ratio for both samples. Excellent agreement was obtained between the modulus measurements from the tensile strain gage, compression strain gage, and crosshead displacement for each sample. The average Poisson's ratio was 0.20 on the tensile and compression sides of the beams. The Poisson's ratio data were extremely consistent for tensile strains ≥0.03% and compressive strains ≤0.03% for both loading and unloading, as shown in Figure 8 for the tensile side of Sample No L22.

Young's modulus values determined by tensile testing and flexure testing were equivalent to one another. However, Poisson's ratio was significantly higher for four-point bend testing (0.20 on tension and compression sides of beam) than for tensile testing (0.07–0.13) or when calculated from the tensile and shear moduli (0.09). The reason for this difference is not known. However, the aspect ratio (loading span/width) of four-point bend Sample Nos. L22 and L23 was low (1.33), which may have affected the Poisson's ratio measurement. The low aspect ratio would introduce stress in the transverse direction because the specimen behaves more like a thin plate rather than a strip between the two loading pins. A small amount of the transverse stress would have a significant effect to the calculated Poisson's ratio. Additional tests on samples with higher aspect ratios could have been performed to address this issue, but was beyond the scope of this investigation.

Table 8. Flexural Modulus and Poisson's Ratio of Samples with Strain Gages

	Flexural Modulus (msi)			Poisson's Ratio	
Sample No.	Tension Gage	Compression Gage	Crosshead Displacement	Tension Gage	Compression Gage
L22	3.56	3.56	3.56	0.17	0.20
L23	3.55	3.57	3.58	0.22	0.19

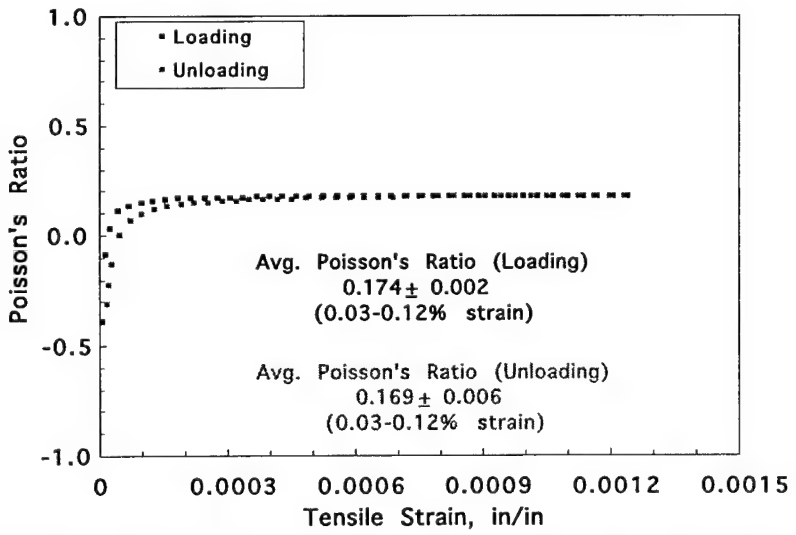

Figure 8. Poisson's ratio on tensile side of four-point bend Sample No. L22.

It is believed that failure initiated on the tensile side of the flexure samples. Therefore, one might expect similar failure strengths for the tensile tests and flexure tests. However, tensile testing at room temperature gave a lower tensile strength (7.32±0.45 ksi) than either four-point (8.88±0.73 ksi) or three-point (11.7±0.7 ksi) bend testing. In principle, tensile and four-point bend loading test larger volumes of material than three-point bend loading since only the area directly under the loading pin is subjected to the peak stress in three-point bending. Furthermore, tensile testing has uniform stresses throughout the gage section, whereas the stress varies through the thickness for both three-point and four-point bending. For a brittle material like Ag/carbon, the measured tensile strength is expected to decrease as the volume of material subjected to the maximum stress increases because the probability of failure occurring at a flaw increases as the volume increases.[2] Therefore, it is not surprising that the strength measured by three-point bending would be greater than that measured by four-point bending, which would be greater than that measured by tensile testing. Tensile testing provides the most conservative strength value.

3.4 Fracture Toughness Testing

The results of the three-point bend fracture toughness tests are summarized in Table 9. An average fracture toughness of 1.56±0.03 ksi(in)$^{1/2}$ was obtained for four samples tested at room temperature. The fracture toughness at room temperature did not depend on the crack depth, and the tests in liquid nitrogen were all conducted with a crack depth of 0.080 in. There was a slight increase in average fracture toughness in liquid nitrogen to 1.67±0.04 ksi(in)$^{1/2}$. Thus, although P-5Ag Ag/carbon is very brittle and sensitive to flaws, flaw sensitivity does not become worse upon cooling to –320°F.

Table 9. Fracture Toughness of Ag/carbon at 72° and –320°F.

Sample No.	Crack Depth (in.)	Failure Load (lb)	Failure Stress (ksi)	F(a/b)	Fracture Toughness (ksi(in)$^{1/2}$)
Three-Point Bend Tests with Cracks at Room Temperature					
L9	0.040	32.2	4.08	1.04	1.51
L10	0.040	33.5	4.29	1.04	1.58
L11	0.080	21.4	2.72	1.14	1.55
L12	0.080	21.7	2.76	1.14	1.58
Three-Point Bend Tests with Cracks in Liquid Nitrogen					
L14	0.080	23.7	3.01	1.14	1.72
L15	0.080	23.0	2.92	1.14	1.67
L16	0.080	22.4	2.87	1.14	1.64
L17	0.080	22.6	2.87	1.14	1.64

3.5 CTE Measurements

The results of the CTE measurements are presented in Figure 9. Plots of $(L–L_o)/L_o$ versus temperature, where L is the sample length at a given temperature and L_o is the length at 72°F are shown over the temperature range of –240 to +210°F. There were no significant differences between the curves for samples cut out parallel to the length, width, and thickness of the as-received P-5Ag rectangular piece. The average CTE for the three measurements was 2.4 ppm/°F, which agrees very well with the value of 2.8 ppm/°F reported by manufacturer.[3]

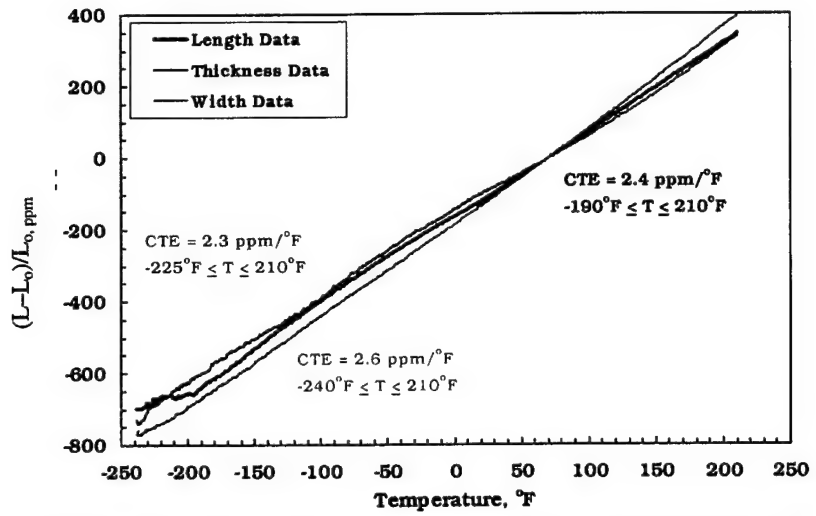

Figure 9. Thermal expansion of Ag/carbon for three orthogonal directions.

3.6 Microstructural Evaluation

A typical micrograph of a polished cross section of P-5Ag Ag/carbon is shown in Figure 10. SEM/EDAX was used to identify the various phases noted on the micrograph. The microstructure consists of a carbon matrix with a second carbon phase and Ag dispersed within the matrix. The very dark contrast regions in the micrograph are voids.

X-ray diffraction was performed to further characterize the microstructure. The X-ray diffraction suggested the presence of two carbon phases, one that was highly ordered and one that was much more disordered. These results suggest that the darker carbon phase in Figure 10 is probably graphite particles and the lighter carbon matrix is a more disordered, possibly glassy carbon phase.

Eighteen separate areas on cross sections of two samples were photographed for the purpose of performing image analyses to estimate the volume fraction of voids. The left side of Figure 11 shows a second area on the same sample as Figure 10. The right side of the figure shows the results of the density analysis to highlight the voids. The red, highlighted area constitutes 16,299 pixels. The total area of the micrograph has 1,976,400 pixels. Thus, the void volume is 0.89 vol.%. The results of the image analysis for all 36 micrographs are presented in Table 10. The porosity was fairly uniform for both samples, varying from a low value of 0.30 vol.% to a high value of 1.46 vol.% for the different areas. The average void volume was 0.7±0.3 vol.%. The porosity is quite low for a carbon matrix composite material. Although we do not know the detailed processing procedures used for P-5Ag, the low void volume and morphology of the Ag phase suggest that Ag was probably introduced into voids in the carbon/carbon matrix.

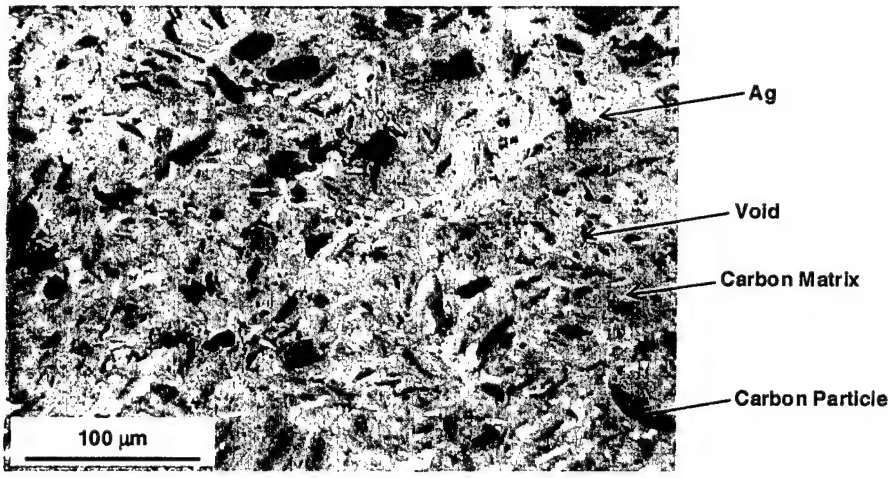

Figure 10. Optical micrograph of polished cross section of P-5Ag Ag/carbon.

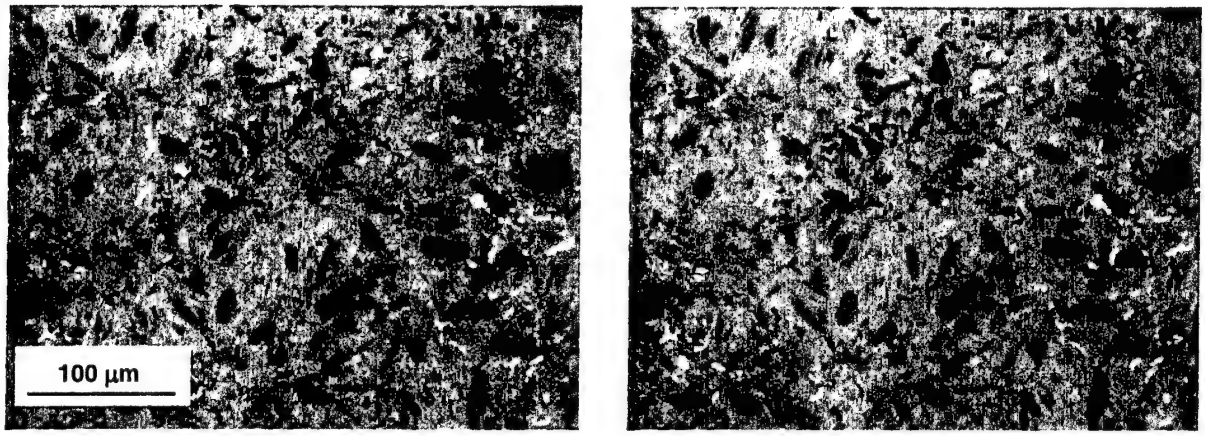

Figure 11. Image analysis of Ag/carbon micrograph highlighting void volume.

Table 10. Void volume by Image Analysis for Two Ag/carbon Samples

Sample No./Area	Void Area (pixels)	Void Vol. (%)	Sample No./Area	Void Area (pixels)	Void Vol. (%)
AGFCTQ4LN/1C	15308	0.77	AGFCTQ2RT/1C	10707	0.54
AGFCTQ4LN/1E	11154	0.56	AGFCTQ2RT/1E	15132	0.77
AGFCTQ4LN/2C	23924	1.21	AGFCTQ2RT/2C	9898	0.50
AGFCTQ4LN/2E	10928	0.55	AGFCTQ2RT/2E	12960	0.66
AGFCTQ4LN/3C	28799	1.46	AGFCTQ2RT/3C	27291	1.38
AGFCTQ4LN/3E	12310	0.62	AGFCTQ2RT/3E	8372	0.42
AGFCTQ4LN/4C	9585	0.48	AGFCTQ2RT/4C	10000	0.51
AGFCTQ4LN/4E	10275	0.52	AGFCTQ2RT/4E	5956	0.30
AGFCTQ4LN/5C	16299	0.82	AGFCTQ2RT/5C	16188	0.82
AGFCTQ4LN/5E	17647	0.89	AGFCTQ2RT/5E	10359	0.52
AGFCTQ4LN/6C	16125	0.82	AGFCTQ2RT/6C	18894	0.96
AGFCTQ4LN/6E	9221	0.47	AGFCTQ2RT/6E	15540	0.79
AGFCTQ4LN/7C	9624	0.49	AGFCTQ2RT/7C	15785	0.80
AGFCTQ4LN/7E	28178	1.43	AGFCTQ2RT/7E	15762	0.80
AGFCTQ4LN/8C	18236	0.92	AGFCTQ2RT/8C	17416	0.88
AGFCTQ4LN/8E	12036	0.61	AGFCTQ2RT/8E	10903	0.55
AGFCTQ4LN/9C	7982	0.40	AGFCTQ2RT/9C	10145	0.51
AGFCTQ4LN/9E	20740	1.05	AGFCTQ2RT/9E	11578	0.59
Average		0.78	Average		0.68
St. Dev.		0.33	St. Dev.		0.25

4. Summary

A test series was conducted to characterize both the room-temperature and the cryogenic-temperature mechanical properties for silver-filled carbon material P-5Ag. The P-5Ag carbon material was procured from Morgan AM&T, Inc. The types of tests in this series included tensile strength, tensile modulus, shear strength, shear modulus, flexure strength and modulus, mode I fracture toughness, and coefficients of thermal expansion (CTE). Specimen configurations included dog-bone-shaped specimens for uniaxial tensile testing, rectangular specimens for flexure and CTE testing, and cylindrical rods for torsion testing and microstructural evaluations. The results of this investigation are summarized as follows.

1. Room-temperature tensile data gave an average tensile strength of 7.32±0.45 ksi. The Young's modulus was calculated to be 3.25 msi. The average –320°F tensile strength was determined to be 7.23±1.54 ksi. The average tensile modulus value at this temperature was 3.18 msi. Thus, there were no significant differences between the tensile properties at 72° and –320°F.

2. Room-temperature shear data gave an average shear strength of 8.32±1.89 ksi. The average shear modulus was 1.49±0.22 msi. At –320°F, the shear strength was 10.95±0.77 ksi, and the shear modulus was 1.49 msi.

3. Since the P-5Ag material is considered as isotropic, the room-temperature Poisson's ratio can be calculated from the Young's modulus and the shear modulus. The calculated Poisson's ratio is 0.09 at room temperature and 0.069 at –320°F. Poisson's ratio determined from biaxial strain gages on a tensile sample tested at room temperature varied from 0.07 to 0.13 as the stress increased.

4. At room temperature, the average flexural modulus was 3.32±0.25 msi for four-point bend tests and 3.16±0.05 msi for three-point bend tests. The average room-temperature strength was 8.88±0.73 ksi for four-point bend and 11.7±0.7 ksi for three-point bend tests. Thus, the flexural modulus was equivalent for three-point and four-point bend tests, but the average flexural strength was 30% higher for three-point than for four-point bend tests.

5. In liquid nitrogen, the average flexural modulus and strength were 2.96±0.37 msi and 12.5±0.8 ksi, respectively, for three-point bend tests. Thus, there were no significant differences between the room-temperature and liquid-nitrogen modulus or strength for three-point bend tests. This is consistent with the tensile test results.

6. An average fracture toughness of 1.56±0.03 ksi$(in)^{1/2}$ was obtained at room temperature. There was a slight increase in average fracture toughness in liquid nitrogen to 1.67±0.04

ksi(in)$^{1/2}$. Thus, although P-5Ag Ag/carbon is very brittle and sensitive to flaws, flaw sensitivity does not become worse upon cooling to –320°F.

7. There were no significant differences in CTE from –240 to +210°F for samples cut out parallel to the length, width, and thickness of an as-received rectangular piece of P-5Ag. The average CTE for the three measurements was 2.4 ppm/°F.

8. Microstructural analyses of P-5Ag indicated that the material consists of two separate carbon phases having differing degrees of graphitization plus a Ag phase. Image analysis showed that the void volume is less than 1 vol.%.

References

1. "Standard Test Methods for Flexural Properties of Unreinforced and Reinforced Plastics and Electrical Insulating Materials," ASTM D 790-96a, *Annual Book of ASTM Standards,* Vol. 8.01, pp. 141–151 (1997).

2. S. B. Batdorf, and D. J. Chang, "On the Relation Between the Fracture Mechanics Statistics of Volume Distributed and Surface Distributed Cracks," *International Journal of Fracture*, Vol. 15, No. 2, April 1979.

3. Morgan AM&T, Inc. Data Sheet, undated.

LABORATORY OPERATIONS

The Aerospace Corporation functions as an "architect-engineer" for national security programs, specializing in advanced military space systems. The Corporation's Laboratory Operations supports the effective and timely development and operation of national security systems through scientific research and the application of advanced technology. Vital to the success of the Corporation is the technical staff's wide-ranging expertise and its ability to stay abreast of new technological developments and program support issues associated with rapidly evolving space systems. Contributing capabilities are provided by these individual organizations:

Electronics and Photonics Laboratory: Microelectronics, VLSI reliability, failure analysis, solid-state device physics, compound semiconductors, radiation effects, infrared and CCD detector devices, data storage and display technologies; lasers and electro-optics, solid-state laser design, micro-optics, optical communications, and fiber-optic sensors; atomic frequency standards, applied laser spectroscopy, laser chemistry, atmospheric propagation and beam control, LIDAR/LADAR remote sensing; solar cell and array testing and evaluation, battery electrochemistry, battery testing and evaluation.

Space Materials Laboratory: Evaluation and characterizations of new materials and processing techniques: metals, alloys, ceramics, polymers, thin films, and composites; development of advanced deposition processes; nondestructive evaluation, component failure analysis and reliability; structural mechanics, fracture mechanics, and stress corrosion; analysis and evaluation of materials at cryogenic and elevated temperatures; launch vehicle fluid mechanics, heat transfer and flight dynamics; aerothermodynamics; chemical and electric propulsion; environmental chemistry; combustion processes; space environment effects on materials, hardening and vulnerability assessment; contamination, thermal and structural control; lubrication and surface phenomena. Microelectromechanical systems (MEMS) for space applications; laser micromachining; laser-surface physical and chemical interactions; micropropulsion; micro- and nanosatellite mission analysis; intelligent microinstruments for monitoring space and launch system environments.

Space Science Applications Laboratory: Magnetospheric, auroral and cosmic-ray physics, wave-particle interactions, magnetospheric plasma waves; atmospheric and ionospheric physics, density and composition of the upper atmosphere, remote sensing using atmospheric radiation; solar physics, infrared astronomy, infrared signature analysis; infrared surveillance, imaging and remote sensing; multispectral and hyperspectral sensor development; data analysis and algorithm development; applications of multispectral and hyperspectral imagery to defense, civil space, commercial, and environmental missions; effects of solar activity, magnetic storms and nuclear explosions on the Earth's atmosphere, ionosphere and magnetosphere; effects of electromagnetic and particulate radiations on space systems; space instrumentation, design, fabrication and test; environmental chemistry, trace detection; atmospheric chemical reactions, atmospheric optics, light scattering, state-specific chemical reactions, and radiative signatures of missile plumes.